ChemComm

Accepted Manuscript

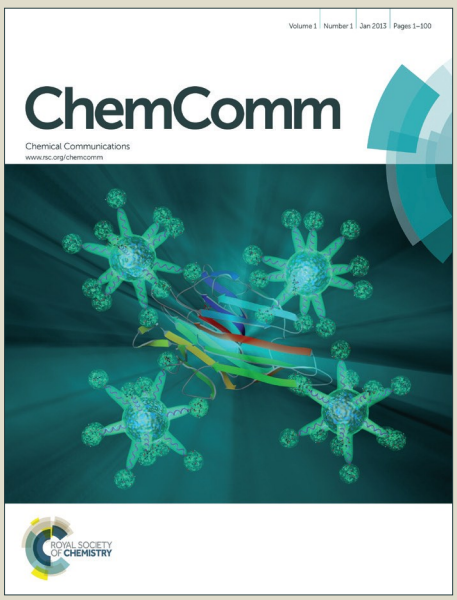

ROYAL SOCIETY OF CHEMISTRY

www.rsc.org/chemcomm

Chem Commun

COMMUNICATION

pH-mediated enhancement of the graphene carbocatalyst activity for reduction of 4-nitrophenol

Received 00th January 20xx,
Accepted 00th January 20xx

DOI: 10.1039/x0xx00000x

www.rsc.org/

Huawen Hu,[a] Xiaowen Wang,[a] Dagang Miao,[a] Yuanfeng Wang,[a] Chuilin Lai,[a] Yujuan Guo,[a] Wenyi Wang,[a] John H. Xin*[a] and Hong Hu*[a]

Using alkaline pH adjustment, the reaction between graphene oxide and L-ascorbic acid led to a carbocatalyst film with numerous graphene edges protruding out of basal planes, which had a markedly enhanced carbocatalytic activity for converting 4-nitrophenol to 4-aminophenol, as compared to that of the carbocatalyst counterpart without involving pH mediation.

To explore and develop catalytic materials capable of replacing precious metal-based catalysts for hydrogenation reactions becomes of increasing scientific importance in order to address many issues correlated with metal-containing species such as rare resource overexploitation and increasing environment pollution caused by heavy metals.[1] In addition, many other problems relating to metal-based catalysts can also be avoided, including metal corrosion, and nanoparticle leaching, poisoning and aggregation resulting from their nano-scale size and high surface energy.[2]

In this regard, metal-free carbocatalysts are the focus of growing scientific and technical interest because they are biocompatible, low-cost, stable, environmentally friendly and readily available.[1b, 3] Graphene materials can be a promising carbocatalyst due to their large specific surface area that offers a large amount of active surface for carbocatalytic reactions. The ultrafast electron mobility of graphene can also make it a decent catalytic material for redox reactions such as chemical reduction of nitro compounds. However, it is challenging to unravel the fundamental mechanism of carbocatalytic reactions over graphene carbocatalysts, especially those prepared by top-down graphite exfoliation using oxidation due to many kinds of active species on the oxygenated graphene, including edges, oxygen functionalities, aromatic π networks and others, which need to be clarified.[1b] Nevertheless, the oxidizing exfoliation of graphite is more suitable for large-scale production and catalytic applications because graphite used as the starting material is available in large quantities from both natural and synthetic sources,[4] and oxygen functionalities and structural defects can be used as catalytic sites for various synthetic transformations.[5]

In this communication, we presented a facile process to enhance the activity of a metal-free graphene carbocatalyst for conversion of 4-nitrophenol (4NP) to 4-aminophenol (4AP), a key synthetic transformation in fine chemical synthesis,[6] through alkaline pH adjustment of the synthetic reaction between graphene oxide (GO) and L-ascorbic acid (AA). Of special interest is a striking contrast between the microstructures formed with and without the pH adjustment under scanning electron microscopy (SEM). In the SEM images, protruding edges of graphene sheets are observable for the carbocatalyst film involving pH mediation and can be correlated closely to a catalytic activity for conversion of 4NP to 4AP. With GO prepared by the oxidizing exfoliation of graphite, the graphene carbocatalysts were synthesized through a mild one-step reaction at room temperature (25 ^{o}C) and with a low AA/GO ratio (1/1). Such a synthetic condition could not make a large change of crystalline structure of GO, with only little impact on the number of the oxygen functionalities existing on the graphene planes as well. Nonetheless, the mild fabrication process can lead to carbocatalyst films showing a certain stability against the present catalytic environment. More interestingly, the microstructure of the film can be modulated by alkaline pH adjustment which exerted large influence on the ionizable carboxyl functionalities. Since carboxyl groups have been reported to be present along the edges, coupled with epoxide and hydroxyl groups on the basal plane of graphene nanosheets,[7] the deprotonation of carboxyl groups allow us to tune the microstructure of the graphene sheets, especially their edges. The present study effectively demonstrates that the deprotonation of carboxyl groups enables the exposing of more active edges of graphene sheets as a result of electrostatic interactions. Of more importance is that more edges exposing could result in a dramatically increased activity for carbocatalytic conversion of 4NP to 4AP. This study may provide insight into the understanding of carbocatalytic reactions over graphene materials as metal-free carbocatalysts, especially hydrogenation reactions.

Fig. 1 schematically presents the fabrication processes of the graphene carbocatalyst films without (pH 4~5) and with (pH 10~11) involving the pH mediation of the starting dispersions containing GO and AA (GO/AA=1/1), which are denoted as carbocatalysts G1 and G2 respectively. The room-temperature synthetic reactions

[a] *Nanotechnology Centre, Institute of Textiles and Clothing, The Hong Kong Polytechnic University, Hong Kong SAR 999077, China*
E-mail: tcxinjh@polyu.edu.hk

† Electronic Supplementary Information (ESI) available: [Experimental section, pH measurements, study on the stability of the carbocatalyst films G1 and G2, investigation of alkaline treatment of the G1 film, XRD patterns, UV/vis spectra, XPS C 1s core-level spectra, SEM observation of the cross-section views of the G1 and G2 films, and catalytic test results involved in using AA, graphite and GO as control catalysts, a recycling test of G2, and others, and SEM observation of the recycled G2 film from the 5th run of catalytic reduction of 4NP]. *See DOI: 10.1039/x0xx00000x*

with AA as a green and mild reducing agent (only composed of C, O, and H) actually exert limited influence on the oxygen groups, π-conjugation structure and crystalline structure of GO, as evidenced by ATR-FTIR, UV/vis, XPS, TGA and XRD characterizations. However, the alkaline pH adjustment can make the deprotonation of carboxyl to carboxylate to a large extent, leading to different pathways of forming the carbocatalyst films. We also found that AA played an important role in the formation of the carbocatalyst films since the absence of AA could only result in the powder sample [Fig. S1 and S2, Electronic Supporting Information (ESI)]. Even though they can be dispersed into water by energy-consuming sonication treatment, the formed films exhibit a stability against shaking or the present catalytic reaction environment, e.g. with reactive $NaBH_4$ as a reducing agent in the catalytic reduction of 4NP to 4AP, in clear contrast to GO powder that can be readily "dissolved" to some extent under simple shaking or in the presence of $NaBH_4$ (insets of Fig. 2-3, and Fig. S3-S4 of ESI). This compact film structure of the carbocatalyst can not only afford its easy recycling but also facilitate the fundamental mechanism analysis of carbocatalytic reactions.

Fig. 2a,b and Fig. 3a,b present similar photo images of the as-formed films G1 and G2 respectively. Under SEM observation, there is also no obvious difference between the cross-section views of the G1 and G2 films (Fig. S5, ESI). We further measured the Brunauer–Emmett–Teller (BET) specific surface area of both the films, and no significant difference can be discerned either (33.8 vs. 36.2 m^2/g). However, their surface microstructures differ greatly under SEM (Fig. 2c and Fig. 3c-3e). The film G1 shows a much more continuous surface, with graphene sheets strongly linked to each other, leaving a limited number of observable separate sheets. By contrast, the film G2 exhibits a significantly more disordered surface structure. A large number of individual graphene sheets can be identified owing to the edges of the graphene sheets, which protrude out of the basal planes. Without involving the pH adjustment, the G1 sheets can be well linked through hydrogen bonding interactions between oxygen groups including carboxyl groups and others. The alkaline pH mediation allows the carboxyl groups to be largely deprotonated, revealing a loss of hydrogen bonding and enhancement of electrostatic repulsion interactions. We also found that, after formation of the G1 film, its post-treatment with an alkaline solution could not lead to conspicuous edges being generated on the G1 film surface (Fig. S6 and S7, ESI), revealing the dependence of the protruding edge formation on the alkaline pH-mediated water-based synthetic reaction with AA.

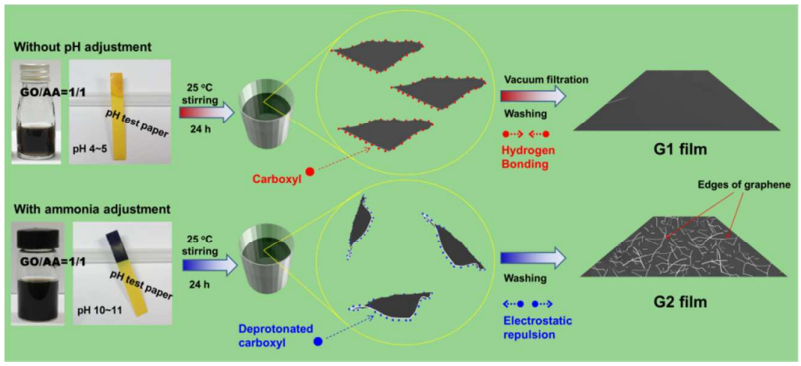

Fig. 1 Schematic illustration of the preparation procedures for carbocatalyst films G1 and G2.

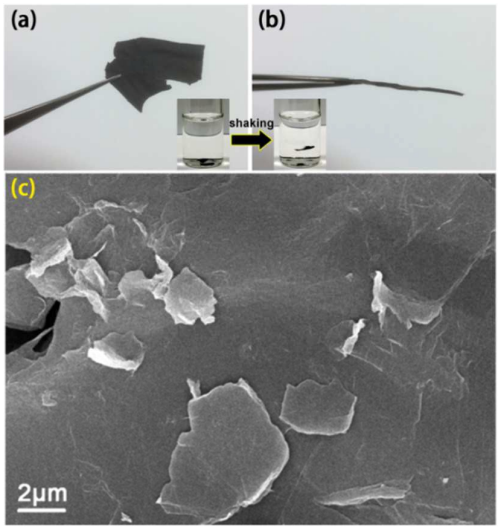

Fig. 2 Photo images and SEM observation of carbocatalyst G1 film. a,b) Photo images showing the top (a) and side (b) views of G1 film. c) SEM images of G1 film. Inset of (a) and (b) shows the G1 film in water under a shaking condition.

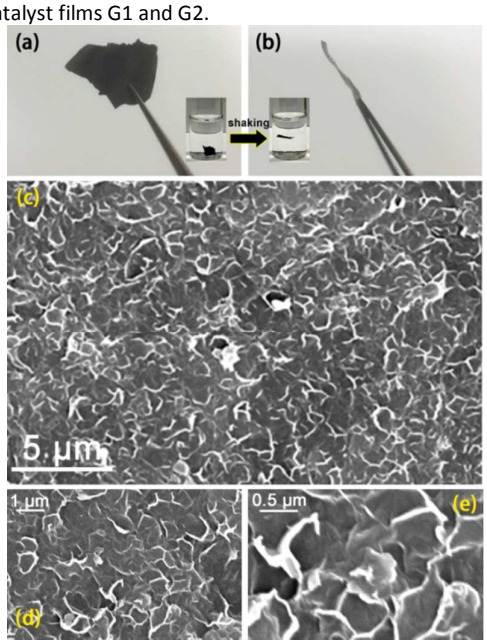

Fig. 3 Photo images and SEM observation of carbocatalyst G2 film. a,b) Photo images showing the top (a) and side (b) views of G2 film. c-d) SEM images of G2 film at different magnification scales. Inset of (a) and (b) shows the G2 film in water under a shaking condition.

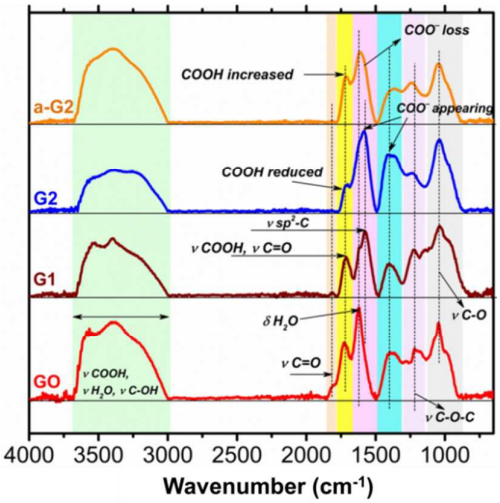

Fig. 4 Normalized ATR-FTIR spectra of GO, G1, G2 and acid-treated G2 (a-G2).

To demonstrate the pH-induced deprotonation of carboxyl groups, ATR-FTIR spectra are provided in Fig. 4. Even though the spectra of GO, G1 and G2 are overall similar, there is indeed partial restoration of the in-plane graphenic structure of G1 and G2 after the reaction between GO and AA, as evidenced by the enhanced absorption at ~1575 cm^{-1} assignable to sp^2-conjugated carbon domain density.[3b, 8] Such restoration can also be confirmed by a slight red shift of the typical UV/vis absorption band from ~233 nm for GO to ~240 nm for both G1 and G2 (Fig. S8, ESI), also indicative of very similar π-conjugation structures in G1 and G2. The weakened FTIR absorption at ~1725 cm^{-1} attributable to carboxyl groups [9] might be an indication of the deprotonation of carboxyl groups of G2 and formation of corresponding carboxylate. The FTIR absorption of carboxylate can result in the spectrum with two prominent peaks at ~1575 and 1405 cm^{-1} which correspond to the asymmetric and symmetric stretching vibrations of the carboxylate respectively.[10] To further determine this deprotonation effect, G2 was treated with hydrochloric acid, so as to protonate the carboxylate and to regenerate carboxyl groups. The acid-treated G2 or a-G2 can indeed show enhanced absorption of carboxyl groups and attenuated absorption of carboxylate, consolidating the pH-induced deprotonation of carboxyl groups of G2 sheets. The carboxyl group deprotonation effect due to the alkaline pH mediation can also be manifested by comparing the pH levels of the dispersions prepared by sonication treatment of G1 and G2 films in water, as shown in Fig. S9 and S10 respectively (ESI). Due to the effective G2 carboxyl deportation, the G2 dispersion shows a little higher pH value (pH ~7), as compared to the G1 dispersion [pH 6~7, close to GO (Fig. S1, ESI)]. Nevertheless, such slightly different alkalinities are unlikely to be the origin of the carbocatalytic activity difference between G1 and G2 films, since our catalytic reaction proceeds in an alkaline condition as a result of the reducing agent $NaBH_4$ involved. The pH levels of the G1 and G2 films (both are close to neutral despite a subtle difference) can be homogenized by the alkaline catalytic environment during the catalysis. As also shown in Fig. S11 (ESI), the pH levels of our catalytic solutions with carbocatalyst films G1 and G2 are basically the same.

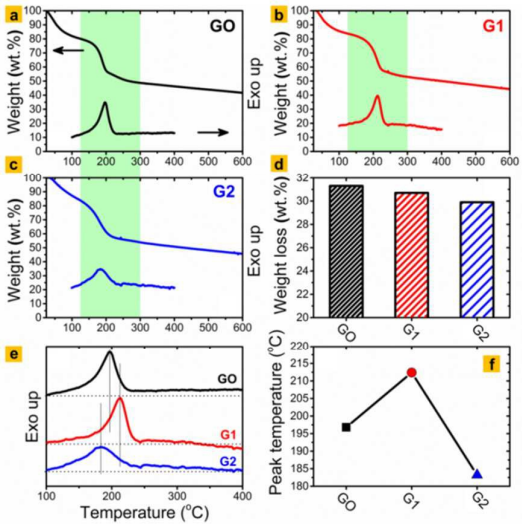

Fig. 5 a-c) TGA coupled with DSC curves of GO (a), G1 (b) and G2 (c). (d) Comparison histogram of the weight loss occurred in the temperature range of 125-300 °C among GO, G1 and G2, as measured from the TGA curves. (e) Stacked DSC curves of GO, G1 and G2. (f) Comparison of DSC exothermic peak temperature among GO, G1 and G2.

Such deprotonation of carboxyl is further demonstrated using TGA coupled with DSC analyses (Fig. 5). The sharp weight loss step in the temperature range of 125 to 300 °C (highlighted by a blue shading) can be found for GO, G1 and G2, attributable to the thermal decomposition of labile oxygen groups.[11] In good consistence with FTIR results, oxygen groups-related weight losses (from the TGA curve) are similar among GO, G1 and G2 (Fig. 5a-5d), with a slightly reduced number of oxygen species after the mild reaction between GO and AA. This can also be confirmed by high-resolution XPS C 1s core-level spectra despite a slightly discernable difference (Fig. S12, ESI). However, DSC patterns are significantly different between G1 and G2 (Fig. 5e and 5f). The exothermal decomposition of the oxygen groups occurs more readily for G2 as compared to that for G1 since a much higher temperature (~213 °C) is needed to start the oxygen group decomposition for G1, as compared to ~183 °C for G2. The deprotonation of carboxyl reduces the hydrogen bonding and enhances the electrostatic interactions between carboxylate, which enables the oxygen groups to be more exposed to heat and thus to be more readily decomposed. Such a deprotonation effect can also be verified through measuring the (001) interplanar spacing of graphite oxide from XRD patterns, as shown in Fig. S13–S15 (ESI). Both G1 and G2 present a crystalline structure similar to that of graphite oxide, revealing that the mild reaction between GO and AA is not capable of changing the crystalline structure of graphite oxide, e.g. to that of a reduced graphene oxide. G1 exhibits a 0.786 nm interplanar spacing as compared to 0.823 nm for G2, indicating that the deprotonation can make G2 sheets more isolated likely due to the electrostatic interactions.

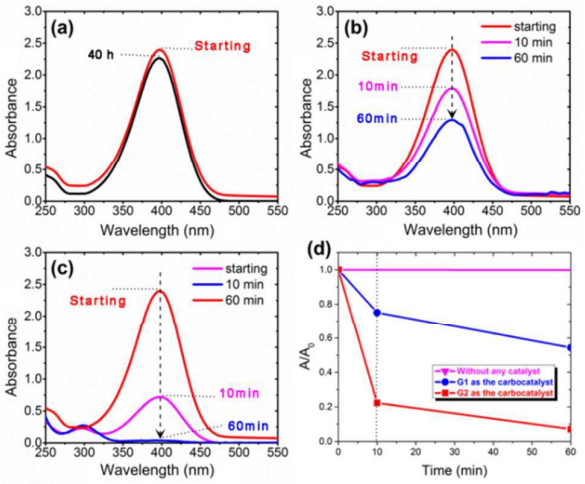

Fig. 6 Catalytic activity test results. a) The reaction between 4NP and BH_4^- without any catalyst. b) Catalytic reduction of 4NP by BH_4^- using G1 as the carbocatalyst. c) Catalytic reduction of 4NP by BH_4^- using G2 as the carbocatalyst. d) Plots of A/A_0 as a function of reaction time for different reaction systems.

A widely-used catalytic reaction model is adopted to measure the activities of G1 and G2, that is, catalytic reduction of 4NP by $NaBH_4$ at room temperature (Fig. 6).[12] Additional catalytic test results are given in Fig. S16-S24 (ESI). If without any catalysts, the reaction between BH_4^- and 4NP can hardly take place, despite the reaction time prolonged to 40 h (Fig. 6a). It took around 60 min to almost disappear completely the adsorption at ~400 nm indexed to 4NP using G2 as the carbocatalyst, accompanied by the emergence of adsorption band at ~300 nm attributable to 4AP,[13] which is much more efficient as compared to the reaction system with G1 as the carbocatalyst (Fig. 6b-6d). This can also be validated by the 4NP solution that is decolorized after the carbocatalytic reaction over G2 for 60 min, whereas a yellow-colored solution can still be observed for the G1-catalyzed reaction system (Fig. S17, ESI). On the other hand, the recyclability of carbocatalyst G2 was also examined, and no significant loss of the G2 activity could be probed after 5 runs of room-temperature catalytic reactions (Fig. S18, ESI). The protruding edges remain conspicuous, which can be an indication of the good recyclability of G2 (Fig. S19, ESI).

For comparison, the catalytic activities of AA, graphite and GO were also measured, but limited activities could be observed (Fig. S20-S24, ESI), although GO powder can be "dissolved" in the catalytic solution to some extent resulting from the reactive $NaBH_4$ and thus has more accessible surface area (Fig. S4 and S24, ESI). The largely enhanced catalytic reaction over G2 relative to that over G1 is most likely ascribed to the protruding edge effect of G2 sheets since other features of the carbocatalyst films G1 and G2 are similar, such as the BET specific surface area, crystalline structure, oxygen group content, and sp^2-conjugated carbon network (Fig. S8, ESI). In addition, it has been theoretically verified that the zigzag edges possess a very high chemical reactivity owing to their special edge states (nonbonding π-electrons) near the Fermi level,[14] and thereby render the graphene-based materials catalytically active, especially the graphene carbocatalyst like G2. Significantly, the present study has presented experimental demonstration that corroborates the theory of the graphene edge effect.

In summary, pH-mediated enhancement of the graphene carbocatalyst activity has been presented for conversion of 4NP to 4AP. We have well demonstrated that the impressively enhanced catalytic activity is correlated closely to the numerous protruding edges of graphene sheets through various characterization analyses. As a consequence, the present study may shed light on understanding carbocatalytic reactions at the molecular level, especially graphene and related materials-catalysed reactions. This work will also provide an impetus towards effectively generating and utilizing the graphene edge effect for many useful synthetic reactions other than the metal-free carbocatalytic conversion of 4NP to 4AP.

We greatly appreciate the PolyU 5316/10E funding from Research Grants Council of the Hong Kong SAR Government.

Notes and references

1. (a) Y. Sun, Y. Wu, H. Shan, G. Wang and C. Li, *Catal. Sci. Technol.*, 2015, **5**, 1290; (b) H. Hu, J. H. Xin, H. Hu, X. Wang and Y. Kong, *Appl. Catal. A: Gen.*, 2015, **492**, 1.
2. (a) D. R. Dreyer, H.-P. Jia and C. W. Bielawski, *Angew. Chem.*, 2010, **122**, 6965; (b) L. Sun, Z. Zhang and H. Dang, *Mater. Lett.*, 2003, **57**, 3874; (c) Q. Wang, B. Zhao, G. Li and R. Zhou, *Environ. Sci. Technol.*, 2010, **44**, 3870; (d) H.-W. Hu, J. H. Xin and H. Hu, *ChemPlusChem*, 2013, **78**, 1483.
3. (a) X.-k. Kong, Z.-y. Sun, M. Chen, C.-l. Chen and Q.-w. Chen, *Energ. Environ. Sci.*, 2013, **6**, 3260; (b) C. Su, M. Acik, K. Takai, J. Lu, S.-j. Hao, Y. Zheng, P. Wu, Q. Bao, T. Enoki, Y. J. Chabal and K. Ping Loh, *Nat. Commun.*, 2012, **3**, 1298 (9pp); (c) S. Navalon, A. Dhakshinamoorthy, M. Alvaro and H. Garcia, *Chem. Rev.*, 2014, **114**, 6179.
4. (a) D. Li, M. B. Muller, S. Gilje, R. B. Kaner and G. G. Wallace, *Nat. Nanotechnol.*, 2008, **3**, 101; (b) H. Hu, C. C. K. Allan, J. Li, Y. Kong, X. Wang, J. H. Xin and H. Hu, *Nano Res.*, 2014, **7**, 418; (c) H. Hu, J. H. Xin and H. Hu, *J. Mater. Chem. A*, 2014, **2**, 11319; (d) H. Hu, J. Xin, H. Hu, X. Wang and X. Lu, *Molecules*, 2014, **19**, 7459.
5. (a) S. Verma, H. P. Mungse, N. Kumar, S. Choudhary, S. L. Jain, B. Sain and O. P. Khatri, *Chem. Commun.*, 2011, **47**, 12673; (b) G. A. B. Gonçalves, S. M. G. Pires, M. M. Q. Simões, M. G. P. M. S. Neves and P. A. A. P. Marques, *Chem. Commun.*, 2014, **50**, 7673.
6. C. Han, Z. Chen, N. Zhang, J. C. Colmenares and Y.-J. Xu, *Adv. Funct. Mater.*, 2015, **25**, 221.
7. O. C. Compton, D. A. Dikin, K. W. Putz, L. C. Brinson and S. T. Nguyen, *Adv. Mater.*, 2010, **22**, 892.
8. Q. Wu, Y. Sun, H. Bai and G. Shi, *Phys. Chem. Chem. Phys.*, 2011, **13**, 11193.
9. J. Pu, Y. Mo, S. Wan and L. Wang, *Chem. Commun.*, 2014, **50**, 469.
10. (a) T. J. Strathmann and S. C. B. Myneni, *Geochim. Cosmochim. Acta*, 2004, **68**, 3441; (b) X. Y. Yang, X. Y. Zhang, Y. F. Ma, Y. Huang, Y. S. Wang and Y. S. Chen, *J. Mater. Chem.*, 2009, **19**, 2710; (c) C. Su, M. Acik, K. Takai, J. Lu, S. J. Hao, Y. Zheng, P. Wu, Q. Bao, T. Enoki, Y. J. Chabal and K. P. Loh, *Nat. Commun.*, 2012, **3**, 1298 (9pp).
11. M. J. Fernández-Merino, L. Guardia, J. I. Paredes, S. Villar-Rodil, P. Solís-Fernández, A. Martínez-Alonso and J. M. D. Tascón, *J. Phys. Chem. C*, 2010, **114**, 6426.
12. (a) H. Hu, J. H. Xin, H. Hu, X. Wang, D. Miao and Y. Liu, *J. Mater. Chem. A*, 2015, **3**, 11157; (b) Y. Zhang, S. Liu, W. Lu, L. Wang, J. Tian and X. Sun, *Catal. Sci. Technol.*, 2011, **1**, 1142.
13. P. Pachfule, S. Kandambeth, D. Díaz Díaz and R. Banerjee, *Chem. Commun.*, 2014, **50**, 3169.
14. (a) T. Enoki, Y. Kobayashi and K.-I. Fukui, *Int. Rev. Phys. Chem.*, 2007, **26**, 609; (b) H. Fu and D. Zhu, *Environ. Sci. Technol.*, 2013, **47**, 4204; (c) G. Lee and K. Cho, *Phys. Rev. B*, 2009, **79**; (d) K. A. Ritter and J. W. Lyding, *Nat. Mater.*, 2009, **8**, 235.